ERS – ENVISAT CROSS-INTERFEROMETRY IN THE ATHENS METROPOLITAN AREA

Ioannis Papoutsis[(1)], Charalabos Kontoes[(2)] and Demitris Paradissis[(1)]

(1) National Technical University of Athens, Dionysos Satellite Observatory , Iroon Polytechniou 9, 15780, Zografou, Athens, Greece, ipapoutsis@space.noa.gr, dempar@central.ntua.gr
(2) National Observatory of Athens, Institute for Space Applications and Remote Sensing, Vas. Pavlou & I. Metaxa, 15236, Penteli, Athens, Greece, kontoes@space.noa.gr

ABSTRACT

In this work, the challenging task of forming cross-interferograms using ERS-ENVISAT Tandem (EET) satellite imagery is dealt with in detail, for the wider Athens metropolitan area. The main focus lies on the interpretation of the coherence map derived by suitable image pairs, in terms of both the imaging geometry and the underlying land cover of the area of interest. Results show that as expected coherence increases in agricultural areas with rolling topography, whereas surface and volume decorrelation kick in for mountainous and urban areas respectively. Additionally for two selected sites that present sufficiently high coherence, one in an agricultural plain and the second in a coastal area, Digital Elevation Models (DEM) are produced from EET pairs and are compared with the corresponding SRTM DEMs.

1. INTRODUCTION

A typical cross-interferogram is formed when an ERS and an ENVISAT/ASAR image are coherently combined. However the 31 MHz difference of the carrier frequency leads to significant spectral decorrelation effects. To compensate for this decorrelation factor one has to take advantage of the spectral shift principle [1] which leads to a requirement for a perpendicular baseline of ~2 km [2] for flat terrain (sign sensitive) to ensure the overlap of the two ground spectra.

The first demonstration of the proof of the above theoretical concept was introduced in [3] for two separate test sites in Las Vegas and Paris. It was immediately recognized that this new interferometric imaging geometry, which allows for very large baselines to be employed, would have an impact on Digital Elevation Model (DEM) reconstruction, by exploiting the increased sensitivity on topographic features (altitude of ambiguity of about 5 m). In conjunction with the very short revisit time of 28 minutes that significantly suppresses temporal decorrelation DEMs were successfully derived in [4] and [5].

The potential to derive accurate DEMs with cross-interferometry (CInSAR) led to a dedicated ERS 2 – ENVISAT tandem mission which was conducted between September 2007 and February 2008, satisfying the perpendicular baseline requirement. However, it was not until recently that a thorough study on DEM generation via CInSAR was introduced [6].

Another important aspect of CInSAR is the study of the statistical behavior of the coherence map derived from the image pair used. In general terms, coherence in CInSAR is affected by a) the perpendicular baseline b) the overlap of the azimuth spectra, c) the underlying topography of the area of interest and d) the land cover type of the imaged scene. Investigation of these parameters and their effect on coherence signature are examined in [7, 8].

For reasons of completeness, although it is not the focus of the present study, it should be mentioned that the possibility to coherently combine ERS and ENVISAT images for PSInSAR applications has also been considered by the research community, introducing an additional term that has to be taken into account when modeling the cross-interferometric phase, that is the Location Phase Screen [9].

The layout of this paper is as follows: firstly the theoretical concepts for CInSAR coherence modeling are formulated, then the SAR data processing specifics are introduced for the Athens metropolitan area, and to conclude the two main results are presented, namely the coherence map analysis and the DEM generation.

2. THEORY ON CInSAR COHERENCE

In conventional InSAR, interferometric phase is mainly affected by geometric and temporal decorrelation. For

Proc. 'Fringe 2011 Workshop', Frascati, Italy,
19–23 September 2011 (ESA SP-697, January 2012)

CInSAR on a tandem mission and ignoring the atmospheric contributions, the image misregistration and thermal noise effects, the general formulation of coherence is given by the following product:

$$|\gamma| = |\gamma|_{geometric} \cdot |\gamma|_{temporal} \quad (1)$$

Geometric decorelation can be decomposed into the three factors that describe the SAR signal scattering mechanism on the ground, i.e. azimuth, surface and volume decorrelation.

$$|\gamma|_{geometric} = |\gamma|_{azimuth} \cdot |\gamma|_{surface} \cdot |\gamma|_{volume} \quad (2)$$

Azimuth decorrelation occurs when the area of interest is imaged with different squint angles between the two acquisitions, leading to different Doppler Centroids and hence partial or no overlap of the corresponding azimuth spectra. Since 2001, ERS-2 has been operating in Zero-Gyro mode leading to continuous variations of the Doppler Centroid along its orbit, making azimuth decorrelation an important parameter that has to been taken into account, via common band filtering techniques. The respective coherence factor is given by:

$$|\gamma|_{azimuth} = 1 - \frac{|\Delta f_{DC}|_{(R_r,R_a)}}{PRF},$$
$$if\ |\Delta f_{DC}|_{(R_r,R_a)} < PRF, else\ |\gamma|_{azimuth} = 0 \quad (3)$$

, where Δf_{DC} is difference in the Doppler centroid and PRF is the Pulse Repetition Frequency. It should be noted that Δf_{DC} is dependent on both the LOS range and azimuth coordinates of the scene.

Surface decorrelation results from the non-perfect overlap of the observed ground range spectra, due to the different observation angles. Surface coherence is given by:

$$\Delta f_{cross} = df - \frac{c \cdot b_n(R_r)}{\lambda \cdot R \cdot \tan(\theta - \alpha)}$$
$$|\gamma|_{surface} = 1 - \frac{|\Delta f_{cross}|}{B_r},$$
$$if\ |\Delta f_{cross}| < B_r, else\ |\gamma|_{surface} = 0 \quad (4)$$

, where Δf_{cross} is the spectral shift defined for CInSAR, df is 31the MHz ERS-ENVISAT frequency difference, c is the speed of light, $b_n(R_r)$ is the range dependent perpendicular baseline, λ is the wavelength, R the distance from the sensor to the center swath, θ is the incidence angle, α the local slope angle and B_r is the processed range bandwidth. To compensate for df, Δf_{cross} should equal zero, which leads to perpendicular baselines of the order of 2 km. If such a baseline is not available, range dependent common band filtering should be performed beforehand, for keeping the common part of the two range spectra. The challenging part is that $|\gamma|_{surface}$ depends on the local slope α, that usually common band filtering does not account for.

Volume scattering occurs when more than one scatterers within a resolution cell contribute to the SAR signal. Assuming a Gaussian distribution of the scatterers, with dispersion σ_z [10]:

$$h_a = \frac{\lambda}{2} \frac{R \cdot \sin(\theta - a)}{b_n}$$
$$|\gamma|_{volume} = 1 - 2\pi^2 \cdot \frac{\sigma_z^2}{h_a^2},$$
$$if\ 2\pi^2\sigma_z^2 < h_a^2, else\ |\gamma|_{volume} = 0 \quad (5)$$

, where h_a is the altitude of ambiguity in meters. Volume decorralation is a significant factor in CInSAR, since the requirement for large compensation baselines leads to a reduced altitude of ambiguity and hence increased sensitivity to height variations within a resolution cell.

The last contributing factor is temporal decorrelation, which is mainly dependent on the land cover type of the scene. In tandem CInSAR with the 28 minutes revisit time, temporal decorrelation is though significantly suppressed.

3. DATA PROCESSING

In the framework of ESA-GREECE AO project 1489OD/11-2003/72, all of the ERS-2 and ENVISAT scenes covering the Athens metropolitan area (Fig. 1) that lies in the prefecture of Attica were acquired.

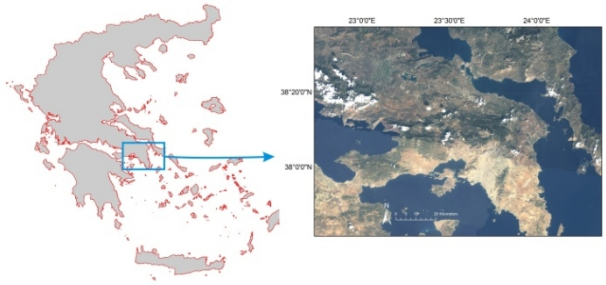

Figure 1. Location of the Athens Metropolitan area within Greece.

Identifying appropriate image pairs for CInSAR that fulfill the criteria for adequate range and azimuth spectra overlap has proven to be a challenging task. To make things worse, the sparse temporal coverage of ENVISAT IS2 acquisitions, due to conflicting requests on ASAR mode of operation, significantly reduces the available dataset for selecting potential SAR pairs.

Despite the above, we were able to extract two image pairs suitable for CInSAR. The details of these two pairs are given in Table I. It should be noted that both the perpendicular baseline and the Doppler Centroid difference shown in this table, were calculated for the center swath of the co-registered scenes.

Two adjacent descending tracks were used, offering increased spatial coverage of the Attica and Evoia regions (total area of 9990 km^2), but with different CInSAR characteristics: while for pair 2 the perpendicular baseline seems to be optimal, for pair 1 it is marginal. Hence it will be interesting to cross-examine the behavior of interferometric phase on both pairs.

Table 1.CInSAR image pairs used

Pair No	1		2	
Orbit No	55200	19328	71461	35589
Sensor	ERS-2	ENVISAT	ERS-2	ENVISAT
Track - Pass	236 - descending		465 - descending	
Date	10/11/2005		20/12/2008	
Perpendicular baseline (m)	1420		1835	
Doppler Centroid difference (Hz)	356		-144	

CInSAR processing of the available scenes was performed with the GAMMA SAR and Interferometry software package [11], going through the following distinct steps:

i. Raw data pre-processing using Delft orbits if available otherwise using ESA DORIS state vectors.
ii. Computation of the Doppler Centroids, accounting for Doppler ambiguities.
iii. Processing of raw data to SLC format, using the nominal Doppler Centroids calculated in the previous step. A criterion in this stage was to keep those pairs whose Doppler Centroid differences were not more than half the azimuth bandwidth, which in this case is half the Pulse Repetition Frequency (PRF ~ 1600 MHz).
iv. Perpendicular baseline estimation using orbital information.
v. Co-registration of multi-looked (5 looks in azimuth) SLCs using an available SRTM DEM of the area. For pair 1 the standard deviations of the model fit used to resample the slave (ERS-2) image to the master (ENVISAT) geometry were 0.0247 and 0.0613 pixel spacing in range and azimuth respectively (i.e. 0.5 m in range and 1.23 m in azimuth), while for pair 2 the same quantities were 0.0183 and 0.036 pixel spacing.
vi. Interferometric processing that consisted of the generation of the initial multi-looked interferogram using common band filtering in range and azimuth, estimation and removal of residual orbital fringes using fringe rate for refining the baseline estimate, and generation of the coherence image.
vii. Phase unwrapping using the Minimum Cost Flow technique and branch-cut algorithm.
viii. Product refinement by 1) estimating any residual baseline components that were not previously accounted for, 2) compensating for residual quadratic phase components and 3) smoothing the interferogram by applying an adaptive (to the fringe rate) spatial filter.
ix. Conversion of the final interferogram to elevation.

4. ERS-ENVISAT COHERENCE

An interesting task is to analyse the patterns evident on the coherence maps derived for the two tandem pairs, in terms of the decorrelation factors presented in section 2. Fig. 2 shows the coherence overlaid with a mosaic of two LANDSAT 5 TM scenes, for pairs 1 and 2.

Examining the behavior of coherence for the two tandem pairs, a general observation is that spatial resolution deteriorates from the eastern (near range for the descending tracks used) to the western (far range) parts of the maps. This is mainly due to the range dependent common band filtering in range and azimuth, performed during the CInSAR processing. In the azimuth direction Fig. 3 depicts the Doppler Centroid variation in range as a function of range samples. Whereas for pair 1 Δf_{DC} increases from near range (225 Hz) to far range (500 Hz), leading to stronger azimuth filtering and hence reduction of the azimuth resolution, for pair 2 it maintains a constant value (~150 Hz).

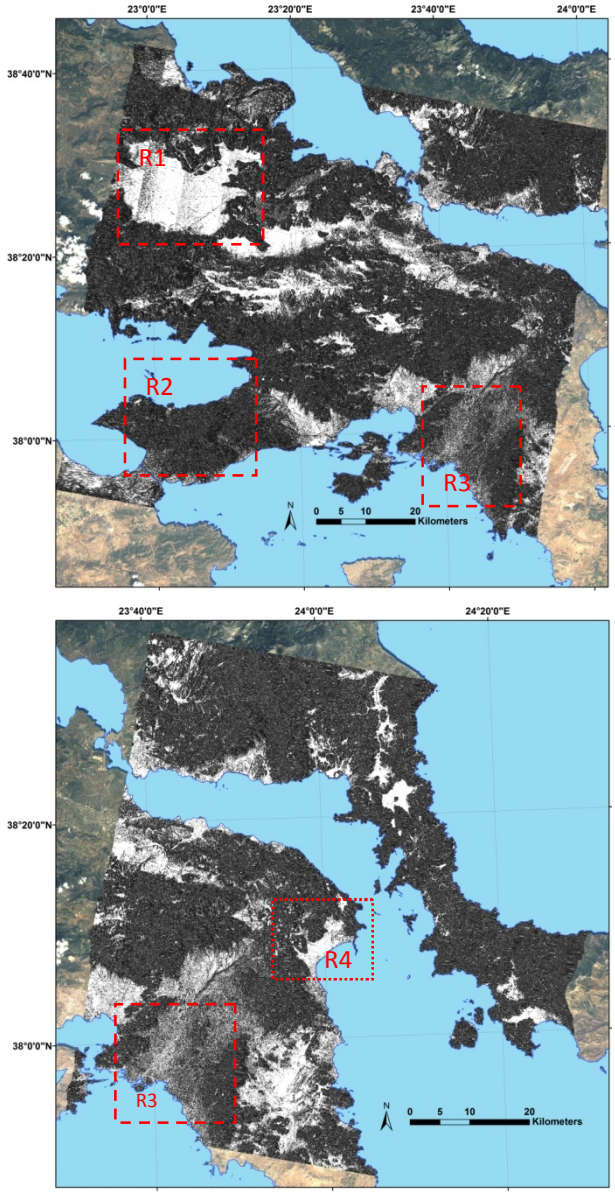

Figure 2.Interferometric coherence for image pair 1 (top) and 2 (bottom). Bright areas correspond to high coherence, whereas dark to low.

The same applies for the resolution in the range direction. Since the perpendicular baseline varies across the swath, the spectral shift defined in Eq. 4 varies with range. The variation of the fractional bandwidth used during range common band filtering is shown in Fig. 4 for the two pairs. Special reference should be made to tandem pair 1 which in the far range the fractional bandwidth was 1.76% with respect to the optimum one (16 MHz), leading to filtering out most of the phase information available. However, still, sufficient coherence was achieved as it can be inferred from investigating region 1 (R1 in Fig. 2). As it will be shown in the following section, this degree of coherence was enough to extract an accurate DEM. Comparing though the common regions of the two coherence maps (eastern part of the top of Fig. 2 and western part of the bottom of Fig. 2), it can be seen that although similar coherence statistics were obtained due to sufficient common band filtering, the spatial resolution of tandem pair 1 is less than that of pair 2.

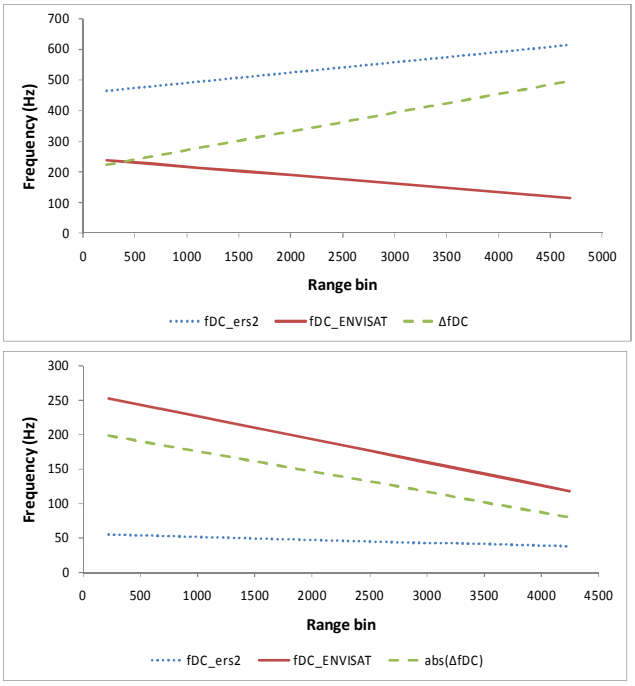

Figure 3. Doppler Centroid variation in range for tandem pair 1 (top) and pair 2 (bottom).

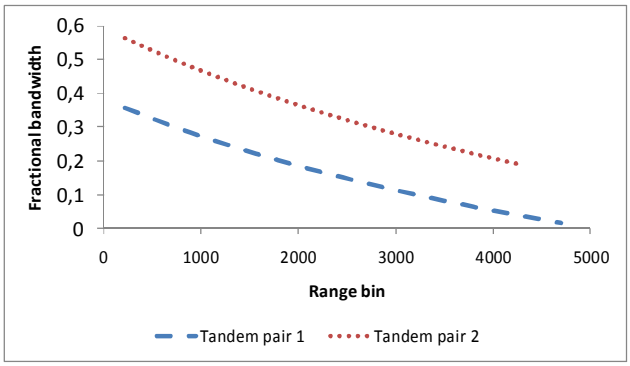

Figure 4. Range variation of the fractional bandwidth used during common band filtering.

Coherence in R1 also reveals a processing shortcoming. One can observe three vertical stripes within which the coherence decreases from right to left in each one of them. This is caused by the fact that the spectral shift was calculated for window stripes of 512 range samples

and therefore common band spatially adaptive filters were applied. This is not optimum for all the 512 range samples, leading to residual band not being common on both SAR scenes. The coherence deterioration is then dictated by surface decorrelation.

Surface decorrelation occurs when common band filtering fails by not taking into account the local slope α in Eq. 4. Coherence as a function of the terrain slope is shown in Fig. 5, for the geometry scenario of pair 1. Region 2 in Fig. 2 contains a mountainous area where interferometric phase is completely incoherent, due to insufficient range spectral overlap.

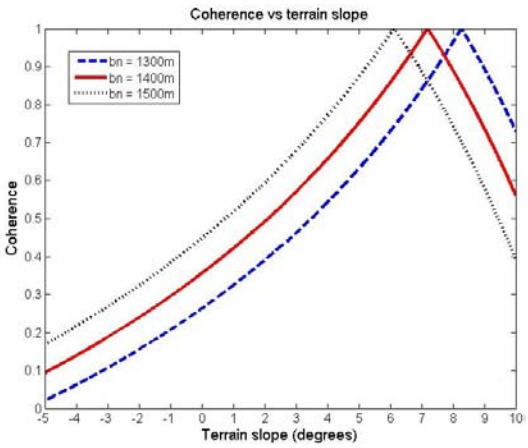

Figure 5. Coherence as a function of terrain slope for different perpendicular baselines. Bn stands for the perpendicular baseline

Volume decorrelation appears to be the dominant factor in region 3 (R3 in Fig. 2) which contains the capital city of Athens. The altitude of ambiguity for pairs 1 and 2 according to eq. 5 is 6.58 m and 5.09 m respectively, assuming flat terrain. This poses a restriction to the height dispersion of the scatterers within the resolution cell to $\sigma_z < 1.24\,m$ and $\sigma_z < 0.95\,m$ correspondingly. It can be confirmed that the urban region in R3 presents low coherence in most parts, due to the above stringent limits. However, there are some clusters of pixels which exhibit strong coherence. These correspond mainly to flat areas and parks within Athens.

In the right part of R3 is located mountain Ymitos where total loss of coherence occurs. This can be attributed to both surface and temporal decorrelation. In fact, the role of temporal decorrelation can be appreciated by considering the underlying land cover of the area of interest. This is presented in Fig. 6, where CORINE Land Cover (CLC 2000) [12] data were used to distinguish between three different classes: artificial surfaces (urban settlements, industrial sites and transport units), agricultural areas (arable land, crop and pastures) and forested areas (all types of forests and shrubs). A direct comparison of Fig. 6 with Fig. 2 demonstrates that vegetated areas are mostly completely decorrelated (the 28' minutes interval proved to be quite long for most types of vegetation), urban areas present moderate to low coherence levels, whereas agricultural areas exhibit high coherence. Typical are regions 1 and 4, where the agricultural geometries derived from CLC 2000 overlap to a great extent with the high coherence areas of Fig. 2. It should be mentioned that the acquisition times of the two tandem pairs were during late autumn – winter seasons, where the phase signature of most crops resembles that of bare soils.

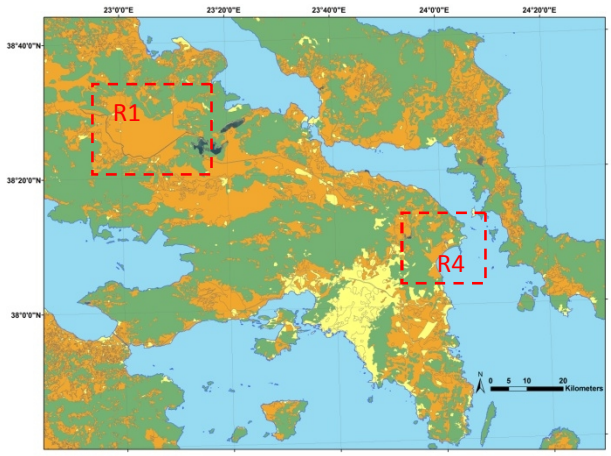

Figure 6.Land cover classes according to CLC 2000. Light yellow corresponds to artificial surfaces, orange to agricultural areas and green to forests and semi-natural areas.

5. DEM GENERATION

The localised nature of regions of high coherence levels, pose a restriction in the generation of a global DEM for the full scene swath. However, in certain scenarios, high accuracy DEMs can be derived for confined coherent areas. The basic concept is to start from a lower resolution DEM, such as an SRTM DEM, and refine the high spatial frequencies from ERS-ENVISAT interferometry. In CInSAR, the value range of the altitude of ambiguity allows for very accurate DEM reconstruction, due to the increased height sensitivity.

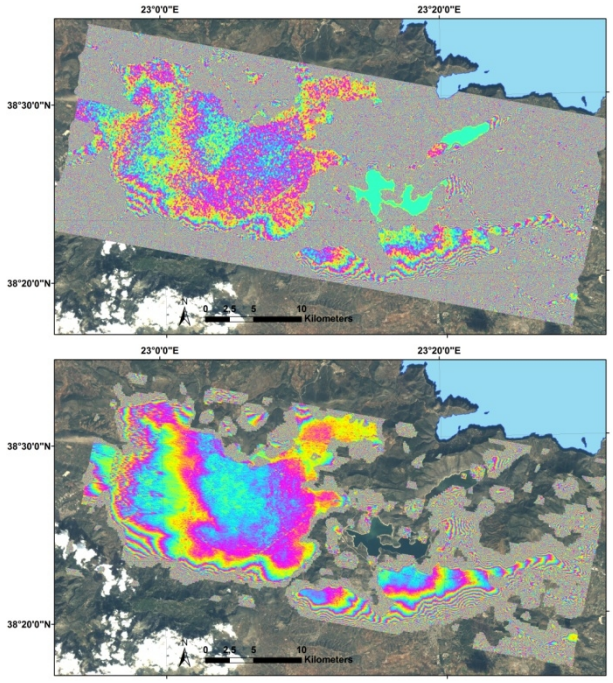

Figure 7.Digital Elevation Model derived from resampled SRTM (top) and CInSAR of tandem pair 1. The color cycle corresponds to 6.5 m.

Two sites were selected to demonstrate the ability to derive accurate DEMs from cross-interferometry, which correspond to R1 (extended to the east) and R4 of Fig. 6. R1 is mainly a rural area covering 1210 km^2. R4, intended to show the applicability of CInSAR to coastal DEM reconstruction, is also agricultural covering 190 km^2. The processing from raw data to phase unwrapping and conversion to height was thoroughly described in Section 3.

In Fig. 7 the CInSAR derived DEM is compared to the SRTM derived DEM for tandem pair 1, while in Fig. 8 the same layout is adopted for tandem pair 2. The SRTM originally with a spatial resolution of 90 m was resampled to 25 m, to match the pixel spacing of the georeferenced DEM originating from SAR imagery. The color cycle for Fig. 7, 8 were set to equal the respective altitude of ambiguities of the two tandem pairs, in order to highlight the height sensitivity of CInSAR. In general, it can be inferred that the same elevation pattern can be recognized in both SRTM and CInSAR DEMs. However the latter is much smoother, underlying the noise reduction capabilities of the technique, in terms of accurate elevation estimation.

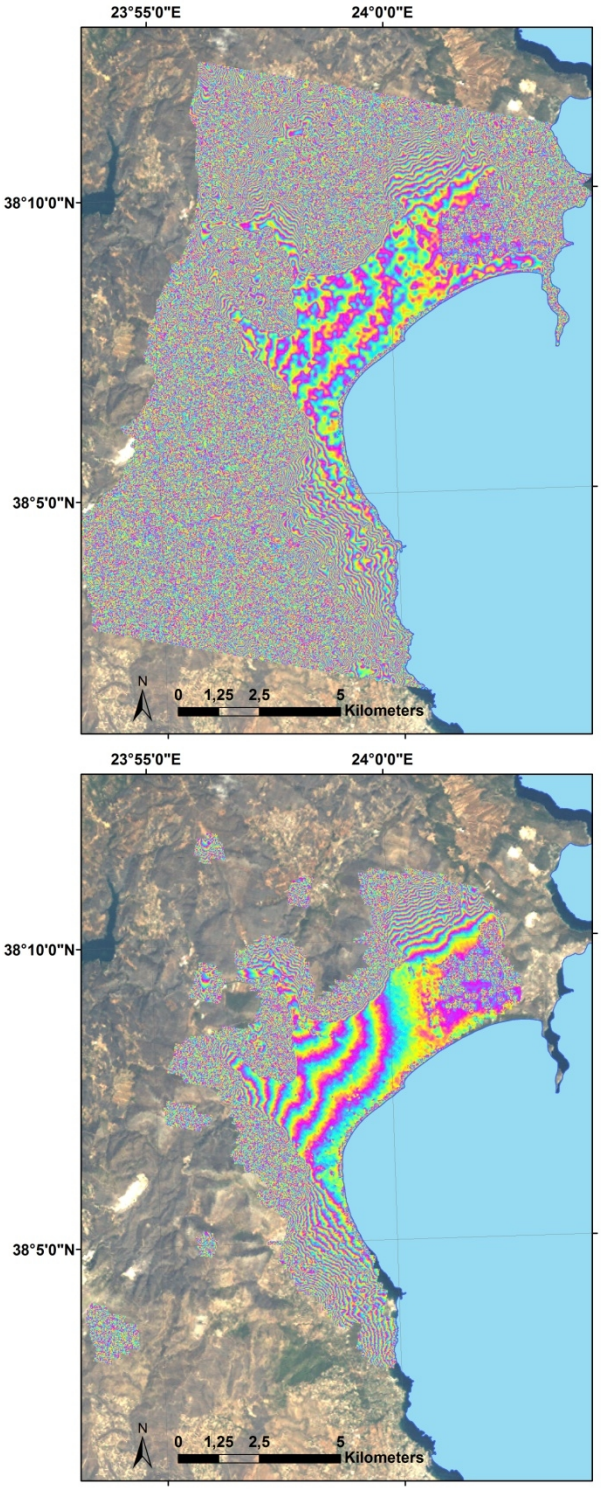

Figure 8.Digital Elevation Model derived from resampled SRTM (top) and CInSAR of tandem pair 2. The color cycle corresponds to 5 m.

6. CONCLUSIONS

Cross-interferometry was demonstrated for two tandem ERS-ENVISAT frames. While for the one tandem pair its perpendicular baseline was close to the compensation baseline, for the second pair it was marginal (~ 1400 m). Under these non-ideal conditions though, CInSAR was achieved, outlining the importance of appropriate, spatially adaptive common band filtering. However this comes at the expense of spatial resolution.

Another important observation was that coherence maps can be used for land use/land cover classification applications. Urban areas were affected by volume decorrelation leading to partial coherence degradation, hilly and vegetated regions exhibited total coherence loss due to surface and temporal decorrelation, and agricultural areas and flat bare soils showed high coherence. Appropriate models of these decorrelation factors though should be generated for the development of an effective classification tool.

Finally, DEM reconstruction was presented for two sites in the Attica area. CInSAR DEM was in agreement with the existing SRTM DEM, significantly suppressing the local height variations of the latter, as a result of the increased height sensitivity offered by the use of long perpendicular baselines. The disadvantage of the method is the reduced spatial coverage of the DEM.

9. REFERENCES

1. Gatelli, F.; Monti Guarnieri, A.; Parizzi, F.; Pasquali, P.; Prati, C.; Rocca, F. The wavenumber Shift in SAR Interferometry. *IEEE Transactions on Geoscience and Remote Sensing* **1994**, 32(4), 855-865.
2. Monti Guarnieri, A.; Prati, C. ERS-ENVISAT combination for interferometry and super-resolution. *ERS – ENVISAT Symposium* **2000**.
3. Arnaud, A.; Adam, N.; Hanssen, R.; Inglada, J.; Duro, J.; Closa, J.; Eineder, M. ASAR ERS Interferometric Phase Continuity. *IEEE Geoscience and Remote Sensing Symposium* **2003**, 2, 1133-1135.
4. Colesanti, C.; De Zan, F.; Ferretti, A.; Prati, C.; Rocca, F. Generation of DEM with Sub-metric Vertical Accuracy from 30' ERS-ENVISAT pairs. *Fringe 03* **2003**.
5. Hong, C.; Wong, J. ERS-ENVISAT Cross-interferometry for Coastal DEM reconstruction. *Fringe 05* **2005**.
6. Wegmuller, U.; Santoro, M.; Werner, C.; Strozzi, T.; Wiesman, A.; Lengert, W. DEM generation using ERS-ENVISAT interferometry. *Journal of Applied Geophysics* **2009**, 69, 51-58.
7. Santoro, M.; Askne, I.H..; Wegmuller, U.; Werner, C.L. Observations, Modeling, and Applications of ERS-ENVISAT Coherence Over Land Surfaces. *IEEE Transactions on Geoscience and Remote Sensing* **2007**, 45(8), 2600-2611.
8. Santoro, M.; Wegmuller, U.; Askne, J.I.H. Signatures of ERS-ENVISAT Interferometric SAR Coherence and Phase of Short Vegetation: An Analysis in the Case of Maize Fields. *IEEE Transactions on Geoscience and Remote Sensing* **2010**, 48(4), 1702-1713.
9. Perissin, D.; Prati, C.; Engdahl, M.E.; Desnos, Y.L. Validating the SAR Wavenumber Shift Principle With the ERS-ENVISAT PS Coherent Combination. *IEEE Transactions on Geoscience and Remote Sensing* **2006**, 44(9), 2343-2351.
10. Ferreti, A.; Monti Guanrieri, C.; Prati, C.; Rocca, F.; Massonnet, D. InSAR Principles – Guidelines for SAR Interferometry Processing and Interpration. *ESA Publications* **2007**.
11. http://www.gamma-rs.ch/gamma.html
12. http://www.eea.europa.eu/data-and-maps/data/corine-land-cover-2000-raster-1